Impact of W on scenario simulations for ITER

G.M.D.Hogeweij[1*], V. Leonov[2], J. Schweinzer[3], A.C.C. Sips[4], C. Angioni[3], G. Calabrò[5], R. Dux[3], A. Kallenbach[3], E. Lerche[6], C. Maggi[7], Th. Pütterich[3], ITPA Integrated Operating Scenarios topical group, ASDEX Upgrade team and JET Contributors †

JET-EFDA, Culham Science Centre, Abingdon, OX14 3DB, UK

[1] FOM-Institute DIFFER, Association EURATOM-FOM, Trilateral Euregio Cluster, P.O.Box 1207, Nieuwegein, The Netherlands, www.differ.nl

[2] IFT, NRC Kurchatov Institute, Moscow, Russia

[3] Max-Planck-Institut für Plasmaphysik, Garching, Germany

[4] European Commission, Brussels, B-1049, Belgium

[5] Associazione EURATOM-ENEA, Frascati, Italy

[6] Association EURATOM-Etat Belge, ERM-KMS, Brussels, Belgium

[7] EURATOM/CCFE Fusion Association, Culham Science Centre, Abingdon OX14 3DB, UK

∗E-mail: g.m.d.hogeweij@differ.nl

Abstract. In preparation of ITER operation, large machines have replaced their wall and divertor material to W (ASDEX Upgrade) or a combination of Be for the wall and W for the divertor (JET). Operation in these machines has shown that the influx of W can have a significant impact on the discharge evolution, which has made modelling of this impact for ITER an urgent task. This paper reports on such modelling efforts. Maximum tolerable W concentrations have been determined for various scenarios, both for the current ramp-up and flat-top phase. Results of two independent methods are presented, based on the codes ZIMPUR plus ASTRA and CRONOS, respectively. Both methods have been tested and benchmarked against ITER-like I_p RU experiments at JET. It is found that W significantly disturbs the discharge evolution when the W concentration approaches $\sim 10^{-4}$; this critical level varies somewhat between scenarios.

PACS numbers: 52.25.Fi, 52.55.Fa, 52.50.Gj

Submitted to: Nucl. Fusion

† *See the Appendix of F. Romanelli et al., Proceedings of the 25th IAEA Fusion Energy Conference 2014, Saint Petersburg, Russia*

1. Introduction - ITER scenario Modelling

Predictions for ITER operating scenarios have been developed for many years [1, 2, 3, 4, 5]. Good progress has been made recently in incorporating particle transport models in scenario simulations for the ITER baseline which has the goal of reaching energy gain $Q = 10$ with ~ 500 MW of fusion [6, 7].

The W level in the ITER core plasma will be determined by many factors. The first factor is the influx through the separatrix, which will depend on the source (divertor sputtering) and which is strongly influenced by the state of the plasma in the Scrape Off Layer (SOL), which can vary from attached to fully detached. The second factor is the transport through the Edge Transport Barrier (ETB), where the relative steepness of electron density (n_e) and ion temperature (T_i) in the ETB can both result in peaked and hollow W profiles [12], and where ELMs can flush W. The third factor is core diffusive and convective W transport, largely determined by the neoclassical component, again strongly dependent on the relative steepness of n_e and T_i. The fourth factor is core MHD; e.g. periodic sawteeth can flush W from the core. For these reasons even a complete and perfect transport model could only predict core W concentrations after several assumptions have been made.

This contribution reports on the impact of including W in the simulations for ITER scenarios, based on the interpretation and extrapolation of results obtained for stable H-mode operation in ASDEX Upgrade and JET [9, 10] and from ITER-like plasma current (I_p) ramp-up (RU) and ramp-down (RD) experiments at JET [11]. The work concentrated on assessing the W content of the core of ITER plasma and the effect of the radiation by W on plasma performance and the evolution of the discharge. Hence for various ITER scenarios the level of W concentration has been determined above which the ITER plasma leaves the allowed or desired operational space, in terms of e.g. l_i, q profile, flux consumption. and energy gain Q. This level will be called the *critical level*. Flux consumption in this paper is always referring the total flux consumption, i.e. the sum of the resistive and inductive contribution.

Because of the many uncertainties affecting core W concentration in ITER, as sketched above, it is attractive to take a pragmatic view. Hence, in stead of carefully modelling W transport from divertor source through SOL, separatrix, ETB into the core, in this paper certain W concentrations have been assumed as given and their effect on the discharge evolution was calculated. This was done in two ways: *(i)* either a given W concentration is assumed for the whole core plasma, *(ii)* or only the W concentration at the separatrix was assumed, in which case simplified transport models were used to predict the core W concentration. The only exception to this will be in section 5.1 on the limiter phase of the I_p RU, where the impurity source (limiter sputtering) is taken into account.

In the realization of ITER scenarios the superconducting poloidal field (PF) coil system plays a crucial role. First, it must provide a stable plasma equilibrium; second, it must be able to provide the significant amount of magnetic flux that is needed to

ramp up the plasma current inductively, and then keep the current flattop phase for a sufficiently long time. The ITER PF coils must remain within several limits, such as coil current, coil field, voltage, power and central solenoid force limits. Allowing for control margins, the PF system of ITER will only allow a range of $l_\mathrm{i} = 0.7 - 1.0$ [8] (note that throughout this paper l_i refers to $l_\mathrm{i}(3)$, as defined in e.g. [8]). Therefore, in the judgement whether a certain W concentration is acceptable, the primary criteria are the value of l_i and the flux consumption.

It is important to include in the predictions for ITER the key observations of the experiments. However, assuming ITER will reach the temperatures expected, basic radiation calculations for high-Z impurities indicate that ITER will be in a different situation from present-day machines; the W radiation is concentrated in the outer half of the plasma, while W radiates in the core at ASDEX Upgrade and JET. Hence results of present-day machines can not be extrapolated to ITER.

The work presented here on scenario simulations for ITER, including the effect of W on the discharge evolution, have been initiated by the Integrated Operation Scenarios Topical Group (IOS-TG) of the ITPA. Within the IOS-TG various methods were applied to achieve this goal. In the present work two methods will be presented and compared, one based on the combination of ZIMPUR and ASTRA, and one base on CRONOS.

The paper is organized as follows: Section 2 briefly summarizes observations of W accumulation in JET and ASDEX Upgrade. Section 3 gives details on the transport codes and models used for the simulations. W accumulation observations in the JET-ILW I_p RU phase have been used to test and benchmark the modelling, which is reported in Section 4. The main part of the paper is then the ITER modelling, as reported in Sections 5 and 6. Finally, in section 7 consequences for future ITER operation are discussed.

2. Summary of experimental results

Recent experiments at ASDEX Upgrade (W limiter and divertor) and JET (W divertor) showed that core W accumulation can have several detrimental effects: a (periodic) loss of the H-mode, as observed in ASDEX Upgrade [9]; strongly perturbed T_e and q profiles during the I_p Ramp Up (RU), as observed in JET [11]; a hollow T_e profile during H-mode, leading to locked MHD modes and finally a disruption in JET [13]. Figure 1 shows examples of W accumulation in JET and ASDEX Upgrade.

The main sources for W and the requirements for controlling the W content of the core plasma have been identified [14]. Comparison between theory and experimental data has shown that, at least in the inner core, neoclassical transport is the dominating contributor to W transport [15, 16]; this result will be used in part of the modelling work discussed in this paper.

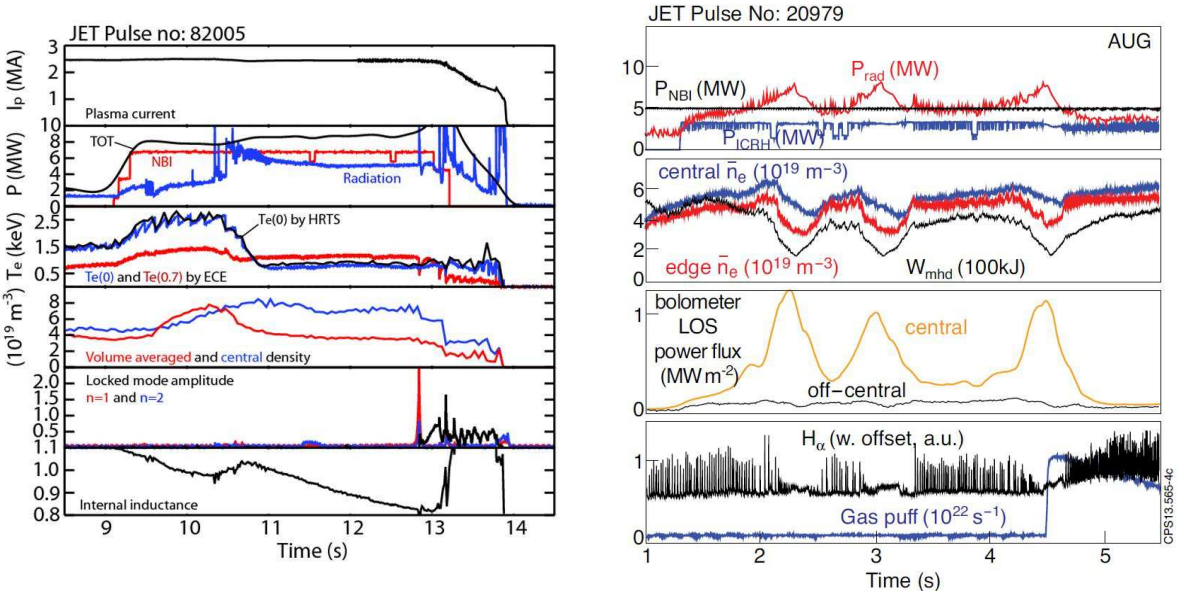

Figure 1. *Examples of W accumulation in JET leading to a hollow T_e profile, locked MHD modes and finally a disruption (left), and in ASDEX Upgrade (right caused a periodic loss of the H-mode (right). Figures taken from [13, 9].*

3. Modelling codes and choices

For the JET simulations n_e profiles, Z_{eff} evolution, and boundary conditions for $T_{e,i}$ and n_e were taken from experimental data. For ITER, these input data were adopted from the ITER team.

All modelling presented is essentially 1D, i.e. poloidal asymmetries are not taken into account; due to the slow rotation of the ITER plasma, centrifugal effects are not expected to be strong.

3.1. ZIMPUR + ASTRA

The first tool used is the combination of the ZIMPUR code [18] for the modelling of impurity behaviour (including neoclassical and anomalous transport for impurities and non-coronal radiation), with ASTRA [19] for the evolution of the bulk plasma parameters.

In ASTRA a scaling based transport model was used. The standard set of transport equations for T_i, T_e, n_d was solved assuming

$$\chi_e = D_d = D_{an} = D_0 \cdot F(\rho) F_H \qquad \chi_i = 2D_{an} \tag{1}$$

where $F_H = 1$ except for the edge barrier region, and the radial profile of transport coefficients was taken of the form:

$$F(\rho) = 1 + 3\rho^2 \quad \text{with} \quad \rho_N = \rho/\rho_{max} \tag{2}$$

The normalization coefficient D_0 was adjusted to provide tau_E as given by the ITER L- or H-mode scalings in the ITER case, or the best possible match of simulated and

experimental radial profiles in the JET case. Convective terms were taken into account in the heat transport equations in the form of $3/2 \cdot T \cdot \Gamma$. For the H-mode cases the external transport barrier region ($\rho_N > 0.93$) was simulated by reducing the factor F_{H} for this region such that

$$\chi_{\mathrm{e}} = \chi_{\mathrm{i}} \simeq {\chi_{\mathrm{i}}}^{\mathrm{nc}} \tag{3}$$

in order to reproduce pedestal profiles.

The transport coefficients used for the different impurity ions are the sum of the anomalous (D_{an}) and neoclassical (NC) contributions. For the latter the total matrix of the NC coefficients for all different ions is used, taking into account collisions between all ions. Production and penetration of W is treated as a 1D process.

3.2. CRONOS

The second tool used is the CRONOS suite of codes [17]. Self-consistent simulations of the I_{p} RU phase were performed both for JET-ILW ITER-like pulses, and for ITER hybrid scenario pulses. Evolution of T_{e}, T_{i} and j were modelled self-consistently.

The semi-empirical Bohm-gyroBohm transport model was used (L-mode version, [20]). In the past this model has proven to give good reproductions of the I_{p} RU phase in JET [21]. See [26] for details. It should be noted that first principles models like GLF23 do not reproduce well the ohmic and L-mode I_{p} RU [21]. Sawteeth were taken into account in the modelling; the Porcelli model was used to describe the sawtooth crash [22]. The radiation was calculated, using detailed atomic physics [23]; the predictions of this model only slightly deviate from the simple average ion model [24].

4. Modelling of the I_{p} RU phase of JET

4.1. ZIMPUR + ASTRA

To benchmark the radiation calculation in ZIMPUR, a JET case with strong W accumulation during the I_{p} RU was modelled predictively (JPN 83444), i.e. the evolution of T_{e}, T_{i} (ASTRA), n_{W} and P_{rad} (ZIMPUR) were simulated, including the external heat sources (5.1 MW of NBI in this case). The inward neo-classical W convection was not strong enough to reproduce the extreme W peaking in this case; therefore the inward convection was artificially enhanced for $\rho < 0.3$. In these simulations the W flux at the boundary was not calculated, but simply chosen to reproduce the correct n_{W} in the core.

Results are summarized in Fig.2. It can be seen that ZIMPUR reproduces quite well the measured P_{rad} profile, and that ASTRA correctly predicts the observed hollow T_{e} profile.

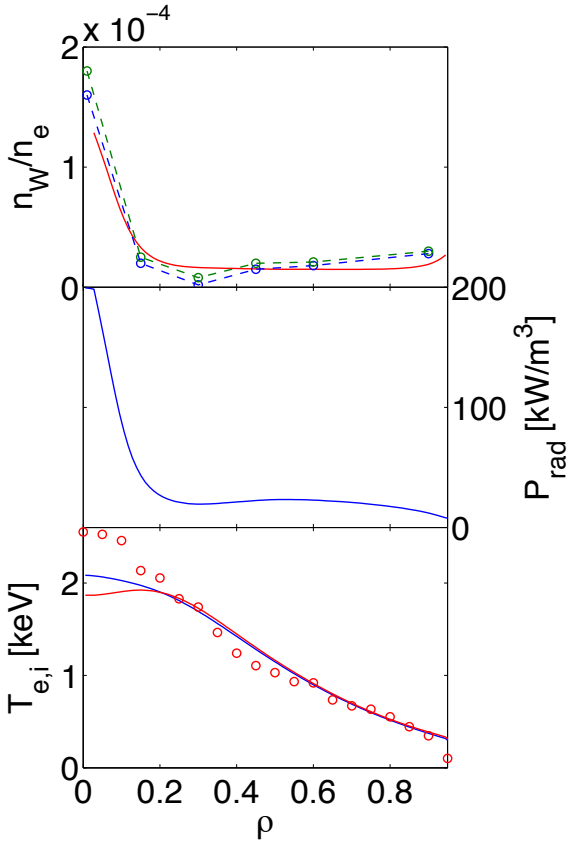

Figure 2. *Profiles of relative W density, radiated power density and* T_e *and* T_i*, as calculated by ZIMPUR+ASTRA, for JPN 83444 at 47s. Full lines: simulation; dashed lines: experimental data.*

4.2. CRONOS

To prepare scenarios for ITER, the discharge evolution during the ITER-like current ramp-up phase in JET was modelled with the CRONOS suite of codes for different W concentrations. In some of these pulses strong W accumulation was observed [25]. The experimental data (T_e, n_e, Z_{eff}) were used. n_W/n_e profiles were assumed either flat or using the same (peaked) shape as measured in the experiments.

Using the experiments as a basis, the W concentration was scanned for the simulations of the current ramp up in JET. A critical W concentration of $\simeq 10^{-4}$ was calculated for an H-mode ramp-up at JET. Also the impact of the shape of the W profile in the plasma was studied. With a flat n_W/n_e (representing cases where the W peaking is controlled), the effect of high W concentration is a global decrease of T_e leading to increased flux consumption, without strong change of the q profile. With a peaked n_W/n_e (core impurity accumulation), above the critical n_W/n_e a hollow T_e profile and reversed shear develop, without strong change of plasma inductance (l_i) or flux consumption. These results are in excellent agreement with experimental findings; for details the reader is referred to [11]. Similar modelling for ASDEX Upgrade is in

progress.

5. Modelling of ITER I_p ramp up and flat top phase with ZIMPUR

5.1. Limiter phase of the I_p RU

Fig.3 shows the calculated evolution of discharge parameters during I_p RU stage of the inductive ITER scenario at $I_p < 7.5$ MA when before X-point formation the plasma column is bounded by a W limiter. In the simulations the plasma column was formed initially near the limiter, which fixed plasma size. Then simultaneously with the I_p rise, the plasma column was shifted to the vacuum vessel center. In this stage bombardment of the limiter by ions accelerated in the limiter sheath potential results in the limiter surface erosion. Limiter sputtering by bulk D/T ions escaping the plasma and self-sputtering by ions of limiter material with different charge on the plasma periphery are the main sources of impurities in the plasma. To estimate the maximum effect, sheath potential reduction due to the secondary electron emission and reduction of the edge plasma temperature due to increase of the particle recycling on the limiter have not been taken into account. Prompt redeposition of W is not taken into account, so the calculated source is an upper limit.

Simulations show that in the early low density I_p RU phase W contamination increases to $\sim 0.05\%$ of n_e and then decreases together with the rise of n_e. The most critical was the phase up to 4-5 s when P_{rad} is near the total power injected into the plasma. On the one hand, radiation of power helps to stabilize boundary temperature on a relatively low level of $\sim 40-50$ eV when limiter sputtering is small (negative feedback). On the other hand, it can impede current rise and at some higher W contamination there is a danger of radiative collapse.

Table 1. Critical relative concentrations of different impurities for the reference ITER scenarios

	W	Ar	Be
Inductive	$\sim 7 \cdot 10^{-5}$	$\sim 2.5 \cdot 10^{-3}$	$\sim 5 \cdot 10^{-2}$
Hybrid	$(2-3) \cdot 10^{-5}$	$(1.2-2) \cdot 10^{-3}$	$(3-4) \cdot 10^{-2}$
Steady State	$(3-3.5) \cdot 10^{-5}$	$(1.8-2.2) \cdot 10^{-3}$	$(8-9.5) \cdot 10^{-2}$

5.2. Flat top

Values of critical impurity concentrations are defined by the available level of auxiliary heating power and accessible Q values. At higher impurity concentrations the discharge parameters (P_{fus} and Q) leave the allowed ITER operational space. Then the power flux through the separatrix drops below the H-L-mode threshold power which induces transition to L-mode with deterioration of confinement and further plasma cooling. Fig.4 demonstrates the dependence of plasma parameters on impurity concentrations for the

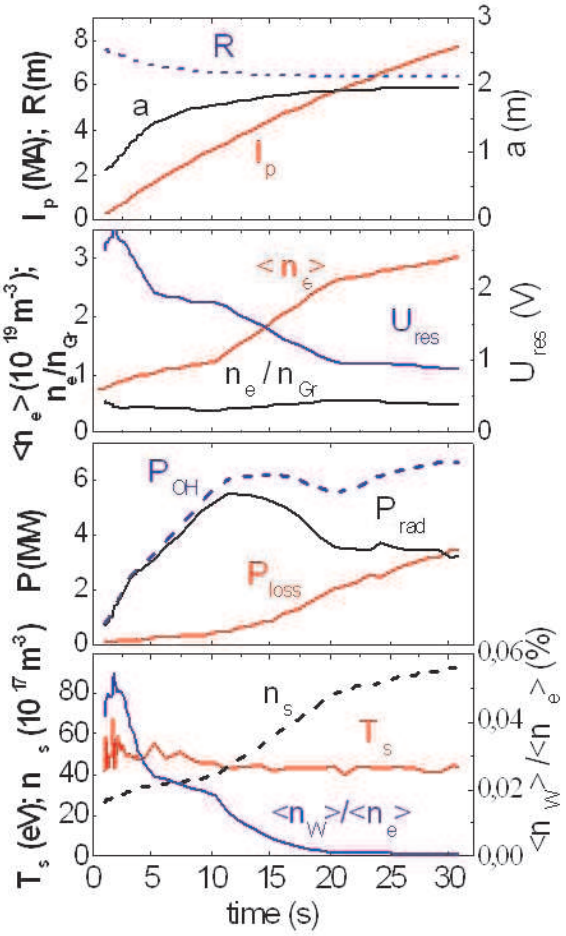

Figure 3. *Evolution of parameters during plasma current ramp-up stage of the inductive ITER scenario with tungsten limiter.*

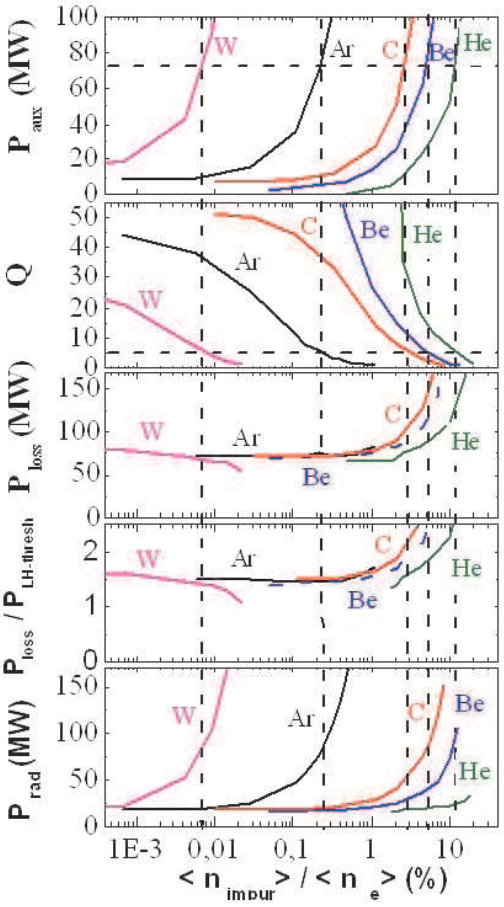

Figure 4. *Change of plasma parameters versus impurities concentrations.*

flat-top stage of the reference inductive ITER scenario. The critical concentrations of different impurities expected for this scenario are found in this figure at $P_{\rm aux} \leq 73$ MW and $Q \geq 5$. Table 1 summarizes estimations for other reference ITER scenarios. For example the calculated critical W concentration ($n_{\rm W}/n_{\rm e}$) is about $7 \cdot 10^{-5}$ for the inductive scenario and a factor of 2-3 lower for the hybrid and steady-state scenarios.

6. Modelling of the impact of W on the $I_{\rm p}$ RU phase of ITER with CRONOS

Second, self-consistent simulations of the $I_{\rm p}$ RU phase for the ITER hybrid scenario were performed with the CRONOS suite of codes. Three different assumptions on the W concentration profile have been used: flat, peaked, and determined by neoclassical transport; each of them will be discussed in the following.

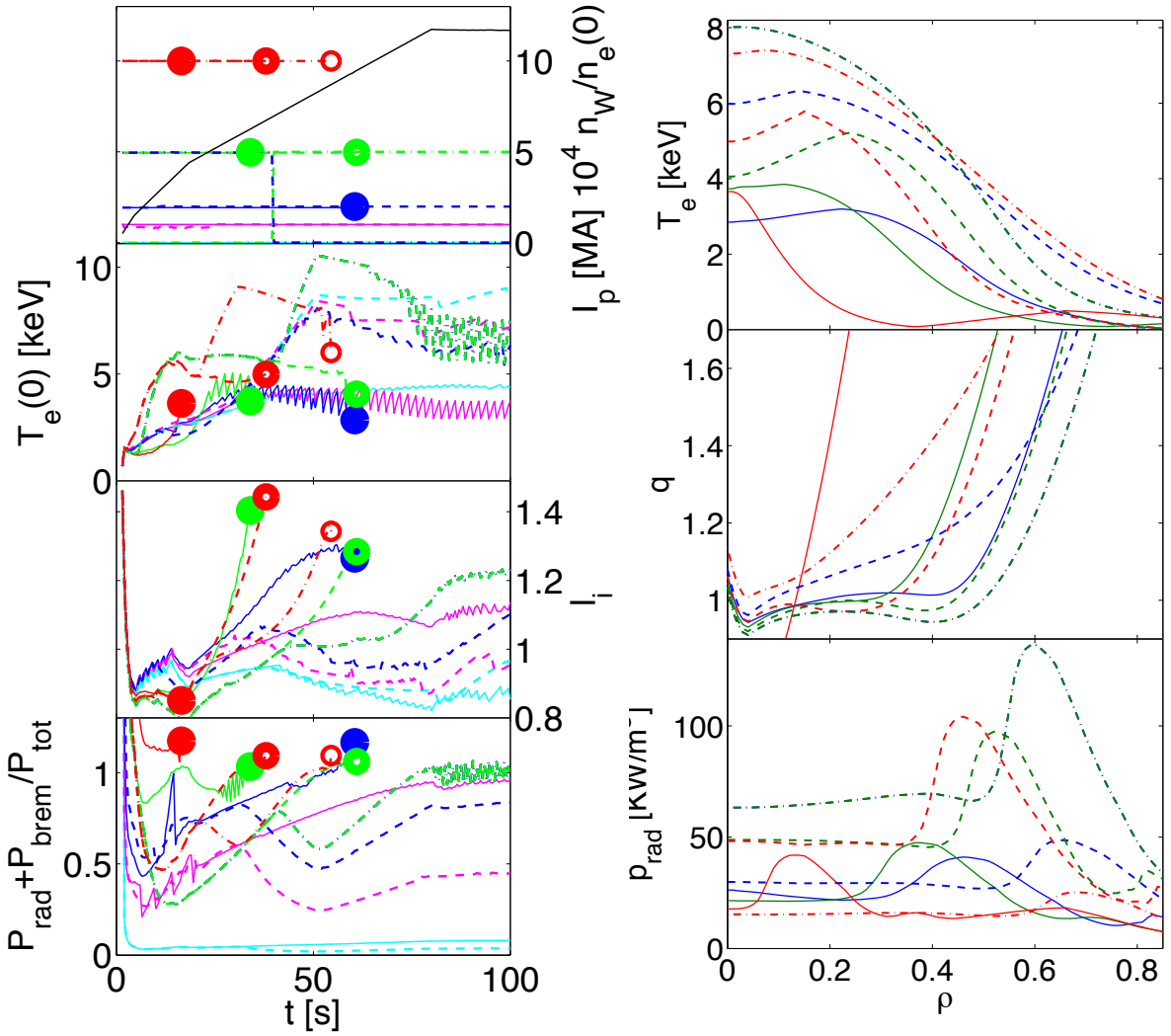

Figure 5. *Results of predictive modelling of various W concentrations, assuming flat n_W/n_e. Shown are ohmic (full lines) and L-mode cases (dashed lines: 20 MW of off-axis ECRH only; dashed-dotted lines: same ECRH plus 20 MW on-axis ICRF). Left panel: time traces of n_W/n_e, $T_e(0)$, l_i, and P_{rad}/P_{in}. In some cases the plasma dies when P_{rad} exceeds P_{in}; these points are marked with a red circle (filled : ohmic; semi-open: L-mode ECRH; open: L-mode ECRH+ICRF). Right panel: profiles of T_e, q and P_{rad} at the end of the I_p RU (80 s), with the same colour coding; in the cases when the plasma dies, the profiles are taken just before the end of the simulation.*

In a first series of simulations, a fixed n_W/n_e concentration was assumed, with a flat profile. Both ohmic and L-mode plasmas were simulated; the latter had, starting at 30 s, 20 MW of off-axis ECH with $\rho_{dep} \simeq 0.5$. For cases with high n_W, also high power L-mode was considered, where in addition to the 20 MW of off-axis ECRH also 20 MW of on-axis ICRF was applied. As seen in Fig.5, for an ohmic ITER ramp-up a flat n_W/n_e profile with $n_W/n_e \geq 1 \cdot 10^{-4}$ leads to unacceptably high l_i. For $n_W/n_e \geq 2 \cdot 10^{-4}$ the plasma dies at a certain moment because P_{rad} exceeds P_{ohm}. However, using 20 MW of

ECRH from early in the ramp-up, the critical level would be increased by a factor of $\simeq 2$; still the plasma dies for $n_{\rm W}/n_{\rm e} \geq 5 \cdot 10^{-4}$ when at a certain time $P_{\rm rad}$ exceeds $P_{\rm ohm}$ + $P_{\rm ECH}$. Adding additional 20 MW of ICRH further enhances these limits by a factor of ~ 2.

6.2. Assuming peaked $n_{\rm W}/n_{\rm e}$ profile

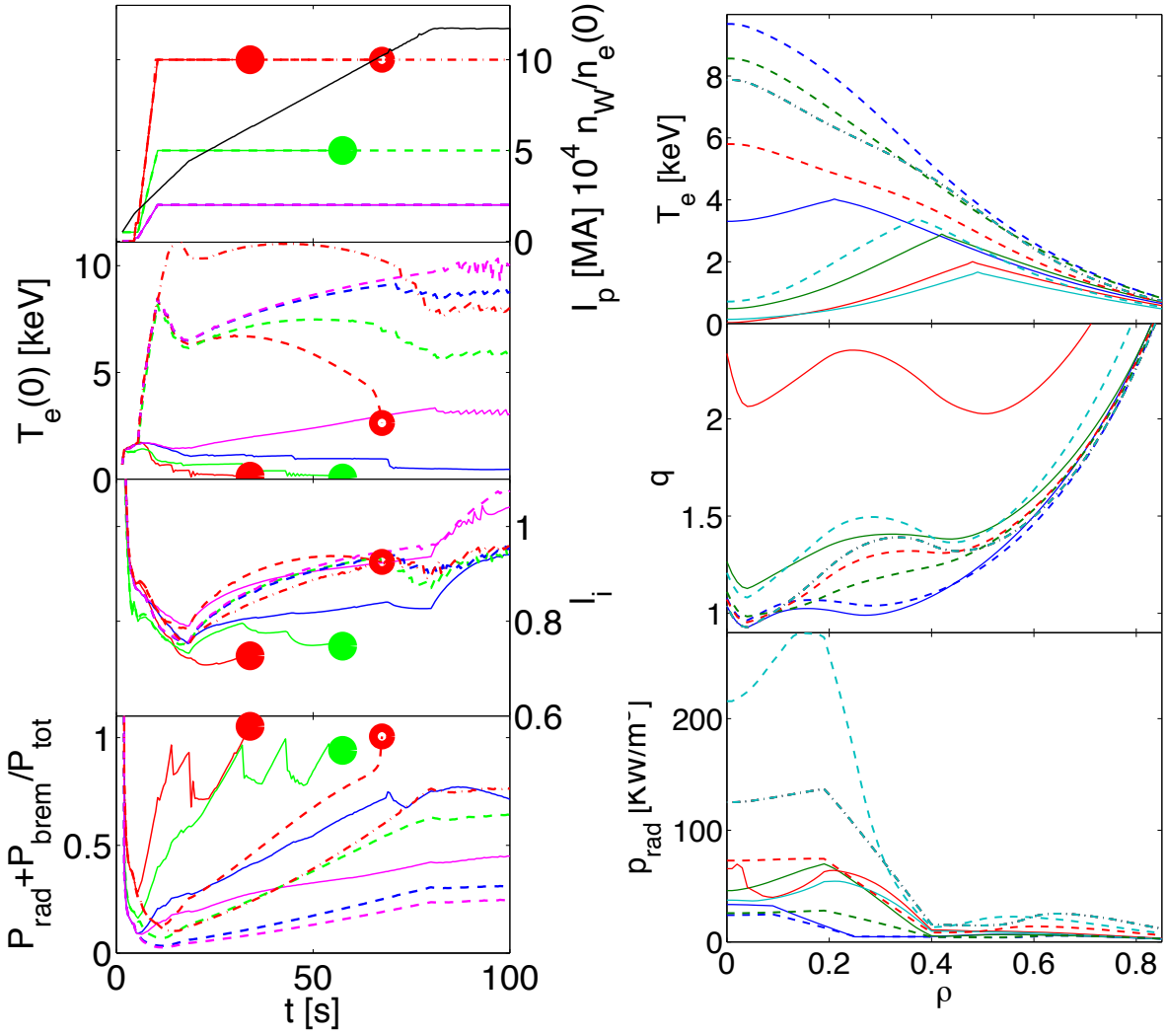

Figure 6. *Results of predictive modelling of various W concentrations, assuming peaked $n_{\rm W}/n_{\rm e}$. Shown are ohmic (full lines) and L-mode cases (dashed and dashed-dotted lines, see previous figure). Left panel: time traces of $n_{\rm W}(0)/n_{\rm e}(0)$, $T_{\rm e}(0)$, $l_{\rm i}$ and $P_{\rm rad}$. Right panel: profiles of $T_{\rm e}$, q and $P_{\rm rad}$ at the end of the $I_{\rm p}$ RU (80 s), with the same colour coding.*

In a second series of simulations, a peaked $n_{\rm W}/n_{\rm e}$ concentration was assumed. Again both ohmic and L-mode plasmas were simulated; the latter had 10 MW of nearly central ECH and in one cases additionally 20 MW of central ICRF. In the simulations a peaking of a factor 5-10 was assumed inside $\rho = 0.15 - 0.4$. With peaked $n_{\rm W}/n_{\rm e}$, there

is no problem with l_i; however, too high central n_W/n_e ($\simeq 2 \cdot 10^{-4}$ in the ohmic case, $\simeq 10^{-3}$ in the L-mode case) causes a net sink in the centre, leading to hollow T_e profiles and perturbed q profiles; see Fig.6.

6.3. Assuming neo-classical core W transport

Finally, in order to have more realistic predictions, a simple W transport model was adopted. There are strong indications that, at least in the inner core, neoclassical transport is the dominating contributor to W transport [15, 16]. If it were the only contributor, one would expect following relation between inverse gradient lengths:

$$1/L_{n_Z^{neocl}} = Z(1/L_{n_i} - F \cdot 1/L_{T_i}) \tag{4}$$

where different values for F are given, e.g. $F \simeq 1/3$ [27] or $F = (Z/2-1)/Z$ [28]. We will use the latter formula, and take $Z = 40$, which is correct for W in the core of JET and ASDEX Upgrade (few keV). For the ITER core (20 keV) $Z = 60$ would be more realistic [23]; however, this will hardly have an effect on the simulation results. It should be noted that Eq.4 is only correct in steady state; n_W will react to changes in n_e and T_i on a neoclassical time scale. In the simulations so far this effect has been neglected. Assuming that the turbulence mechanisms governing particle transport are the same for all species, it is sensible to assume

$$n_W{}^{turb} \sim n_e \tag{5}$$

Due to the high Z value, Eq.4 could yield extremely hollow or peaked n_W in the inner core. Residual turbulent transport and MHD will make these profiles less extreme; hence we assume in the inner core n_W to be a combination of $n_W{}^{nc}$ and $n_W{}^{turb}$, which leads to:

$$\begin{aligned} &\text{for } \rho \geq \rho_{bd} : n_W = n_W{}^{turb} = \gamma \cdot n_e \\ &\text{for } \rho \leq \rho_{bd} : n_W = \zeta\gamma \cdot n_e + n_W{}^{nc} \\ &\text{where } n_W{}^{nc}(\rho_{bd}) = (1-\zeta)\gamma \cdot n_e(\rho_{bd}) \end{aligned} \tag{6}$$

where $n_W{}^{nc}$ obeys Eq.4, and the match of the first two formulas of Eq.6 at ρ_{bd} yields the last formula. In the simulations we take

$$\gamma = 10^{-4} \qquad \zeta = 0.5 \qquad \rho_{bd} = 0.4 \tag{7}$$

The crucial point is the peakedness of the n_e profile. We will assume three parabolic shapes with low, medium, high and very high peaking factor $n_e(0)/\langle n_e \rangle = 1.3, 1.47, 1.57$ and 1.66, respectively. The latter may seem unrealistically high; however, it should be noted that scaling studies predict a peaking factor of $\simeq 1.5$ for ITER, due to its low collisionality [29].

Simulation results are summarized in Fig.7, both for cases with constant n_e peaking and for cases with low initial n_e peaking and higher n_e peaking in the later ramp-up phase. If no additional heating is applied during the I_p RU, then

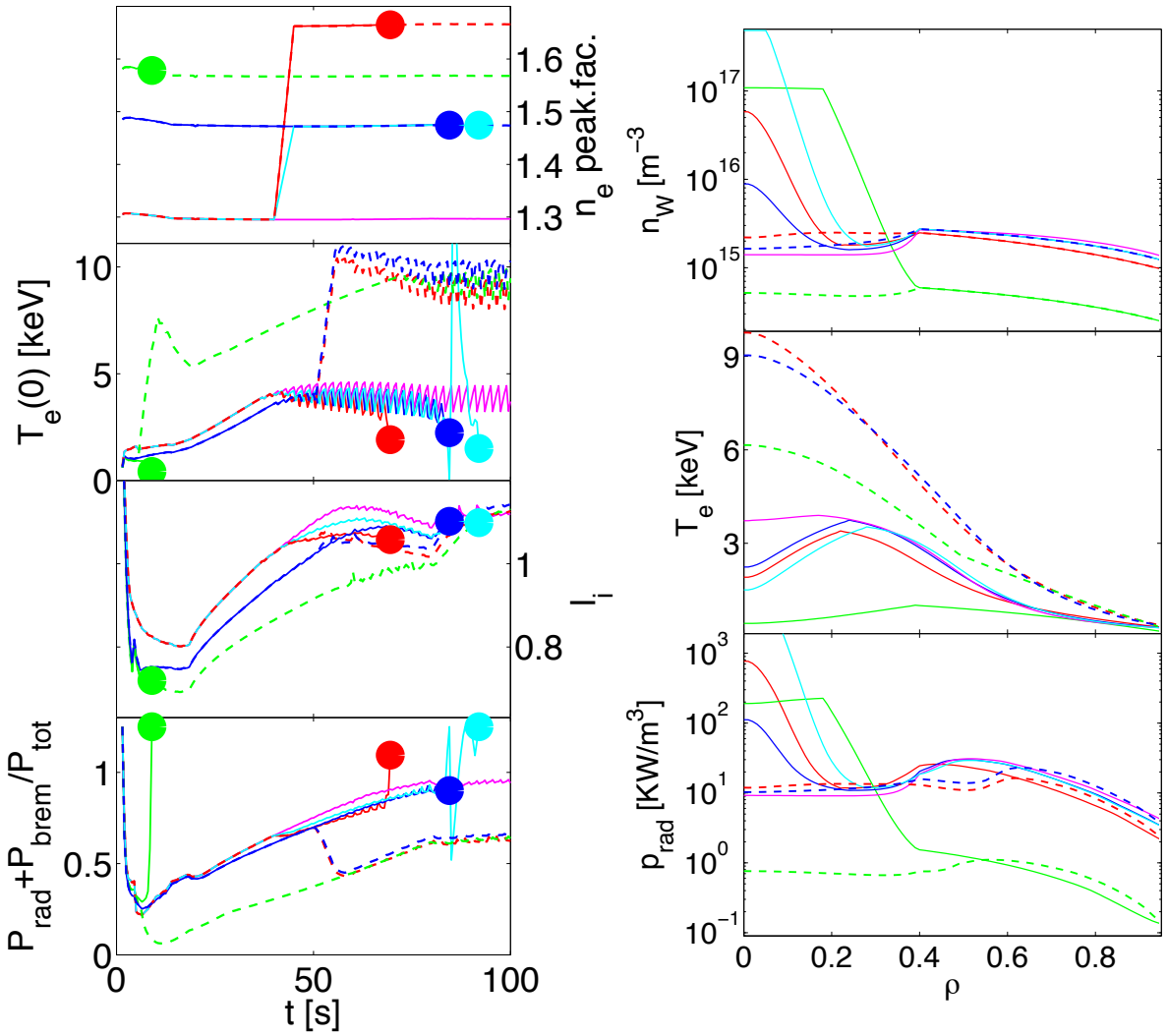

Figure 7. *Results of predictive modelling with $n_{\rm W}$ prescribed by Eqs.6,7. Shown are ohmic (full lines) and L-mode cases (dashed line). Left panel: time traces of $n_{\rm e}$ peaking, $T_{\rm e}(0)$, $l_{\rm i}$ and $P_{\rm rad}$. Right panel: profiles of $n_{\rm W}$, $T_{\rm e}$ and $P_{\rm rad}$ at the end of the $I_{\rm p}$ RU (80 s), or just before the plasma dies, with the same colour coding. Note the logarithmic scale for $n_{\rm W}$ and $P_{\rm rad}$.*

- The case with low density peaking yields a hollow $n_{\rm W}$ profile.
- In the intermediate case, $n_{\rm W}$ is well controlled during the ramp-up; however, soon after the $I_{\rm p}$ RU the plasma dies due to a sudden W peaking.
- In the peaked case the plasma dies already after 9 s due to extreme W peaking.
- When the density becomes peaked halfway the $I_{\rm p}$ RU, the plasma survives for at least 30 s before strong W peaking sets in.

In all cases, additional 10 MW centrally deposited ECRH is sufficient to keep the plasma healthy. If $n_{\rm e}$ becomes suddenly more peaked during the $I_{\rm p}$ RU, then there is sufficient time left to switch on ECRH: in the simulations ECRH was switched on 10 s after the $n_{\rm e}$ peaking started, and this was sufficient to keep the plasma healthy.

6.4. L-H transition

The available auxiliary power in ITER (ECRH, ICRH, NBI) is expected to be only marginally above the L-H threshold power ($P_{\rm LHthr}$), which is expected to be near 50 MW [30]. As the critical parameter for the L-H transition is the heat flux through the separatrix, a significant amount of core radiation would mean that $P_{\rm LHthr}$ can not be attained. Fig.8 shows, both for ohmic and L-mode $I_{\rm p}$ RU, $P_{\rm rad}$ as function of line averaged $n_{\rm W}(0)/n_{\rm e}(0)$ for the case of flat (left) and peaked (right) $n_{\rm W}/n_{\rm e}$ profiles at 60 s, i.e. at 3/4 of the $I_{\rm p}$ RU. In the latter case $n_{\rm W}/n_{\rm e}$ is inside $\rho = 0.25$ assumed to be a factor of 10 larger than outside. As can be seen, $P_{\rm rad}$ rises more or less linearly with $n_{\rm W}/n_{\rm e}$, and for $n_{\rm W}/n_{\rm e} \simeq 210^{-4}$ one has $P_{\rm rad} \simeq 10$ MW, which can be considered as a significant fraction of $P_{\rm LHthr}$.

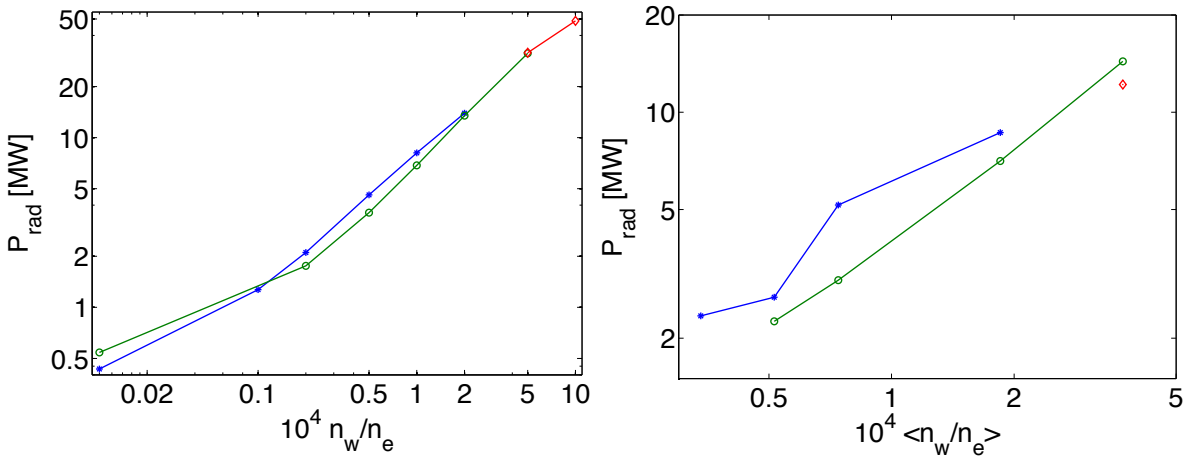

Figure 8. *$P_{\rm rad}$ as function of line averaged $n_{\rm W}(0)/n_{\rm e}(0)$ for the case of flat and peaked $n_{\rm W}/n_{\rm e}$ profiles (left, right, respectively) at 60 s, i.e. at 3/4 of the $I_{\rm p}$ RU(80 s) for ohmic (blue), L-mode with ECH only (green), and L-mode with both ECH and ICRF (red).*

6.5. Flux consumption

Also the increased flux consumption due to W accumulation is a point of concern. The inductive flux will not change much; there only the resistive flux consumption will be considered. Fig.9 shows the resistive flux consumption up to 60 s as function of $n_{\rm W}/n_{\rm e}$, for various heating schemes. For a given heating scheme a W concentration if 210^{04} causes an increase of flux consumption by 20-30 Vs. Given the typical loop voltage in the flat-top of 0.02-0.04 V, this would mean that the projected flux consumption of the whole flat-top would already be consumed in the $I_{\rm p}$ RU phase. On the other hand, the red points in the plots from cases with extremely early switch-on of strong auxiliary heating (30-40 MW of ECRH plus ICRF from 10 s) show that such a heating scheme would reduce flux consumption to the normal level (i.e. without W accumulation).

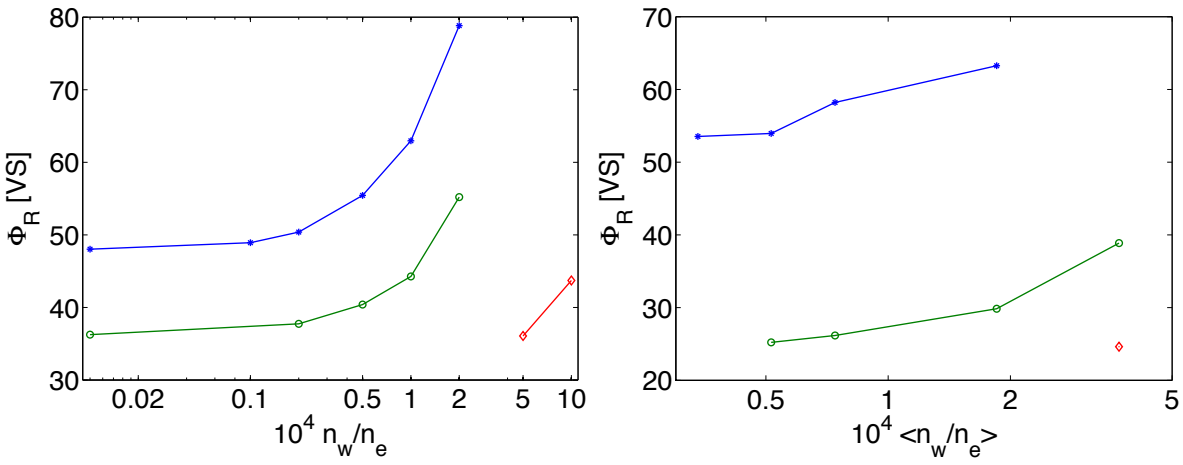

Figure 9. *Resistive flux consumption up to 60 s as function of line averaged* $n_{\mathrm{W}}(0)/n_{\mathrm{e}}(0)$ *for the case of flat and peaked* $n_{\mathrm{W}}/n_{\mathrm{e}}$ *profiles (left, right, respectively), for ohmic case (blue), for L-mode with 10/20 MW ECH from 40 s (green), and for L-mode with 30-40 MW of additional power (ECH plus ICRF) already from 10 s (red).*

7. Conclusions and Outlook

Critical W concentrations have been determined, both for the I_{p} RU phase and for the flat-top phase of various ITER scenarios, using two different suites of codes: first ZIMPUR plus ASTRA, second CRONOS. Both were successfully tested against experimental JET data. The results of the different codes are consistent.

For the ohmic I_{p} RU phase, the critical W concentration is a few times 10^{-5}; with 10-20 MW of additional heating this limit is enhanced by a factor of $\simeq 2$. For maintaining $Q > 5$ at 15 MA in ITER the W concentration should be below $7 \cdot 10^{-5}$.

Apart from assuming certain n_{W} concentrations (flat or peaked), also the assumption of the n_{W} profile being fully determined by neo-classical transport was exploited. the latter assumption leads to an extreme sensitivity of the n_{W} profile on the peaking of the n_{e} and T_{i} profiles. This sensitivity was also found for simulations of n_{W} profiles in the ETB, which may vary from very peaked to very hollow [12].

As critical W concentrations have now been calculated for different ITER scenarios, future work can concentrate on further quantify these limitations. For this purpose the maturing understanding of neoclassical and anomalous W transport, taking into account the effects of poloidal asymmetries [16], will be used.

References

[1] Kessel C.E. *et al* 2007 *Nucl. Fusion* **47** 1274
[2] Parail V. *et al* 2009 *Nucl. Fusion* **49** 075030
[3] Budny R.V. *et al* 2009 *Nucl. Fusion* **49** 085008
[4] Citrin J. *et al* 2010 *Nucl. Fusion* **50** 115007
[5] Kritz A.H. *et al* 2011 *Nucl. Fusion* **51** 123009

[6] Zagórski R. *et al* 2011 *J. Nucl. Mat.* **415** S483
[7] Ivanova-Stanik I. *et al* 2014 *Contr. Plasma Phys.* **54** 341
[8] A.C.C. Sips *et al* 2009 *Nucl. Fusion* **49** 085015
[9] Neu R. et al., *IEEE Tr. Plasma Science* **42** (2014) 552
[10] Beurskens M.N.A. et al., *Plasma Phys. Control. Fusion* **55** (2013) 124043
[11] Hogeweij G.M.D. et al., *Nucl. Fusion* **55** (2015) 013009
[12] Dux R. et al., *Plasma Phys. Control. Fusion* **56** (2014) 124003
[13] De Vries P.C.et al., *Phys. Plasmas* **21** (2014) 056101
[14] Van Rooij G.J. et al., *J. Nucl. Mat.* **438** (2013) S42
[15] Angioni C. et al., 40th EPS Conf. on Plasma Physics (2013) P4.142
[16] Angioni C. et al., *Nucl. Fusion* **54** (2014) 083028
[17] Artaud J.-F. et al., *Nucl. Fusion* **50** (2010) 043001
[18] Leonov V.M. et al., *Plasma Phys. Control. Fusion* **47** (2005) 903
[19] Pereverzev G.V. et al., *ASTRA: Automated System for Transport Analysis in a Tokamak*, Max-Planck Institute Report, IPP 5/98
[20] Erba M. et al., *Nucl. Fusion* **38** (1998) 1013
[21] Imbeaux F. et al., *Nucl. Fusion* **51** (2011) 083026
[22] Porcelli F. *et al* 1996 *Plasma Phys. Control. Fusion* **38** 2163
[23] Th. Pütterich *et al* 2010 *Nucl. Fusion* **50** 025012
[24] D. Post. et al, At. Data Nucl. Data Tables 1977 **20** 397
[25] G. Calabrò *et al*, 40th EPS Conf. on Plasma Physics (Espoo, Finland) 2013, O2.106
[26] Hogeweij G.M.D. et al., *Nucl. Fusion* **53** (2013) 013008
[27] Mantica P. et al., *Trans. Fusion Sc. and Techn.* **53** (2008) 1152
[28] Helander P., SIGMAR D.J., *Collisional Transport in Magnetized Plasmas*, 2002, Cambridge University Press
[29] Weisen H. et al., *Nucl. Fusion* **45** (2005) L1
[30] Doyle E.J. et al., *Nucl. Fusion* **47** (2007) S18

Acknowledgements

This work was supported by EURATOM and carried out within the framework of the European Fusion Development Agreement. The views and opinions expressed herein do not necessarily reflect those of the European Commission. This work is supported by NWO-RFBR Centre-of-Excellence on Fusion Physics and Technology (Grant nr. 047.018.002).